

## Overview: In which dynamic trajectories of molecules are described using rate equations

Much of our discussion of the interplay of the molecules and macromolecular complexes that fill the cell, both large and small, has been founded upon the use of arguments about chemical potentials and equilibrium constants. In living cells, however, circumstances are constantly changing. Ion channels are constantly opening and closing, enzymes are constantly catalyzing biochemical transformations, and the elements of the cytoskeleton are growing and shrinking. In this chapter, we introduce deterministic and statistical approaches for handling these kinds of dynamical processes within cells. In particular, this chapter introduces the use of rate equations, which provide a description of the time variation of populations of different chemical species. We illustrate these ideas with special reference to the dynamics of ion channels, enzyme kinetics, and cytoskeletal assembly.

“Mathematics is biology’s next microscope, only better; biology is mathematics’ next physics, only better.”

**Joel Cohen**

### 15.1 Biological Statistical Dynamics: A First Look

A cell is a bustling metropolis of chemical reactions that are linked together in complex networks of reactants and products. Whether we think about the chemical reactions that make up the metabolic pathways that guarantee the energy solvency of living cells such as are shown in Figure 5.2 (p. 191) or about the synthetic pathways that construct the structural components of such cells, ultimately, all of these pathways are built up of chemical reactions. If we measure the chemical activity of living cells, we see that the rates and identities of these reactions are constantly changing to reflect the dynamics of metabolism, cell division, and motility, to name a few examples. As

a result, we are faced with the challenge of putting together modeling tools that are up to the task of describing the rich dynamics of cellular life.

Thus far in this part of the book, we have considered the fluid dynamics of life's watery medium and the diffusive dynamics of random walks in sparse and crowded environments. To truly tackle biological dynamics, we must also consider transformations in which a molecule changes its identity rather than just its position. We begin by examining a few case studies in cellular dynamics and then derive the mathematical toolbox to address these problems quantitatively.

### 15.1.1 Cells as Chemical Factories

When we first considered the composition of cells in Chapter 2, we estimated the average cell contents in terms of the numbers of each of the kinds of macromolecular component. For a review, see Section 2.1.2 on p. 38. In deriving the average values, we paid no attention to the biological reality that every cell and every component within it is in a constant state of material flux. As cells go about their daily business of consuming, excreting, growing, dividing, moving around, etc., their compositions are constantly changing. Even for a cell under fairly constant conditions, which is not actively changing in size, its individual constituents are constantly being synthesized and degraded in a steady-state manner. When conditions do change, living organisms rapidly adapt by altering their complement of proteins, RNAs, lipids, other macromolecules, and even small metabolites.

Examples of the variation in cells over time at the level of the genes that are expressed were shown in Figures 3.23 (p. 119) and 3.25 (p. 121). It is technically more difficult to measure changes in protein, lipid, or metabolite levels than it is to measure changes in RNA levels, but many such experiments have indeed shown that the compositions can vary to a surprising degree over a very short time. In order to quantitatively understand the nature of these changes, we must be able to describe the processes by which one kind of chemical species is transformed into another. The general theme of transformation is embodied over many different time scales and size scales in living cells. Rapid transformations can include processes such as protein phosphorylation and steps in metabolic pathways catalyzed by enzymes. Slower transformations may include the construction of new large-scale assemblies such as the bundles of stereocilia at the top of an inner ear hair cell during differentiation. Because cells usually contain many copies of each individual kind of molecule, it is often useful to think of transformations at a population scale as changes in concentrations. Accordingly, several of our derivations will consider rate problems as descriptions of changes in concentrations over time. However, ultimately, the transformations so conveniently characterized in terms of concentrations are nothing but time-varying reactions of molecules. One of the main goals of the chapter will be to integrate the molecular-level and population-level views of rate equations.

In order to give a feeling for the numbers with respect to rates of biological transformations, we consider an everyday example, literally the amount of energy that is used by the human body every day.

**Estimate: Rate of ATP Synthesis in Humans** To get a sense of the cellular ATP budget, consider the ATP equivalent of the average daily human diet of 2000 kcal. If we use an approximate figure of 12 kcal/mol as the energy liberated by the hydrolysis of ATP and further assume that half of the energy input in the form of our diet is turned into ATP, the number of moles of ATP synthesized each day is equal to  $(1000 \text{ kcal/day})/(12 \text{ kcal/mol}) = 80 \text{ mol/day}$ . Given that the molecular weight of ATP is roughly 500 g/mol, this implies a daily turnover of more than 40 kg of ATP! Obviously a human body does not at any moment have 40 kg of ATP; this mass reflects the constant turnover accompanying metabolic processes. A total of 40 kg of ATP is synthesized as part of this busy metabolic enterprise.

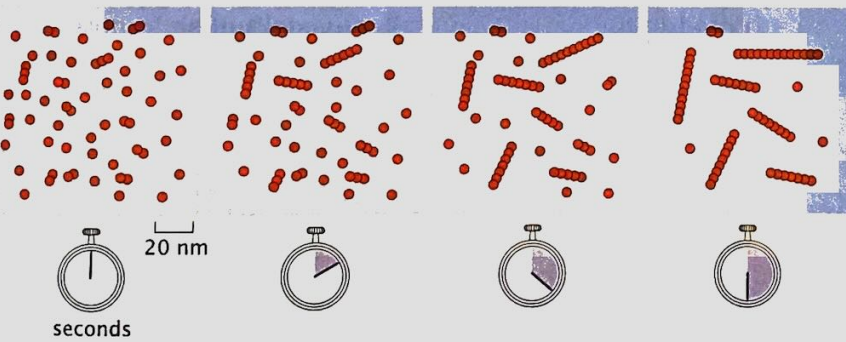


### 15.1.2 Dynamics of the Cytoskeleton

In addition to the constant flux of small metabolites of the cell such as ATP, there is also a surprising degree of turnover among the cell's structural elements. We have already considered the filaments of the cytoskeleton in a number of contexts, for example, as macromolecular assemblies in Chapter 2, as beams that can bend and buckle in Chapter 10, and as one of the key elements that make the cell so crowded in Chapter 14. However, we have neglected to explore the construction of these filaments and their extraordinarily dynamic nature.

All cytoskeletal polymers within living cells are constantly growing and shrinking by addition and loss of protein subunits at the same time as they are serving as construction beams and tracks for molecular motors. The rates of the process of filament assembly are

(A) *in vitro* polymerization



(B) *in vivo* polymerization

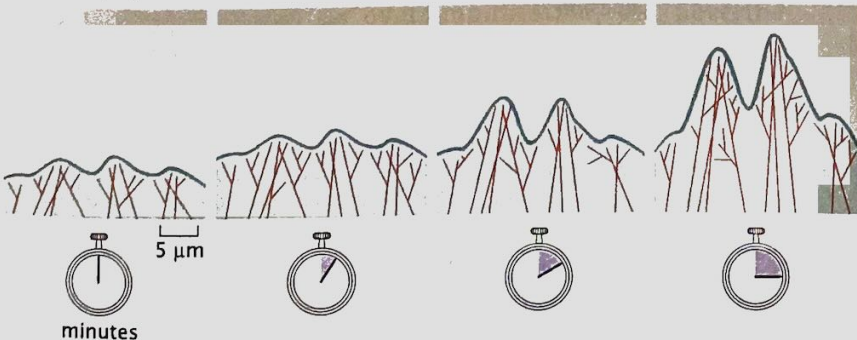


**Figure 15.1:** Snapshots in the life history of cytoskeletal filaments. These schematics aim to give a sense of the spatial and temporal dynamics of cytoskeletal assembly. (A) *In vitro* assay revealing the growth of cytoskeletal filaments assembled from monomeric subunits. (B) *In vivo* time series showing the dynamics of actin filaments growing at the leading edge of a crawling cell.

illustrated in Figure 15.1 for actin filament assembly both *in vitro* and *in vivo*. *In vitro*, a solution of purified actin monomers can assemble into filaments over a time scale of a few minutes. In cells, this same kind of assembly over comparable time scales can be harnessed to push forward the leading edge of a crawling cell. The microscopic processes that attend polymerization are more complex than those shown here. For example, subunits can dissociate from the filaments as well as assemble, and in addition there are ATP hydrolysis reactions that take place within the polymer. Furthermore, the rate at which monomers are added to the growing filament depends upon the concentration of actin monomers and also on the regulatory influences of many other proteins in the cell.

The rates associated with cytoskeletal dynamics can be estimated by observing the motions of living cells. Figure 15.2 shows a fish skin cell called a keratocyte migrating on a surface. Note that actin filaments are polymerizing at the leading edge of the cell and pushing the membrane forward with the cell moving at an average rate of  $0.2 \mu\text{m/s}$ . Interestingly, this same fundamental process of orchestrated cytoskeletal assembly can be hijacked by infectious bacteria such as *Listeria monocytogenes* and used as the basis of their own motility within the cytoplasm of the infected human host cell as shown in Figure 15.3. In this case, the bacterium manipulates the host cell cytoskeletal self-assembly process to form a comet tail made up of actin filaments that pushes the bacterium along at rates ranging between  $0.05$  and  $1.4 \mu\text{m/s}$ , depending upon the host cell type. As shown in Figure 15.3(C), the key components of this system can

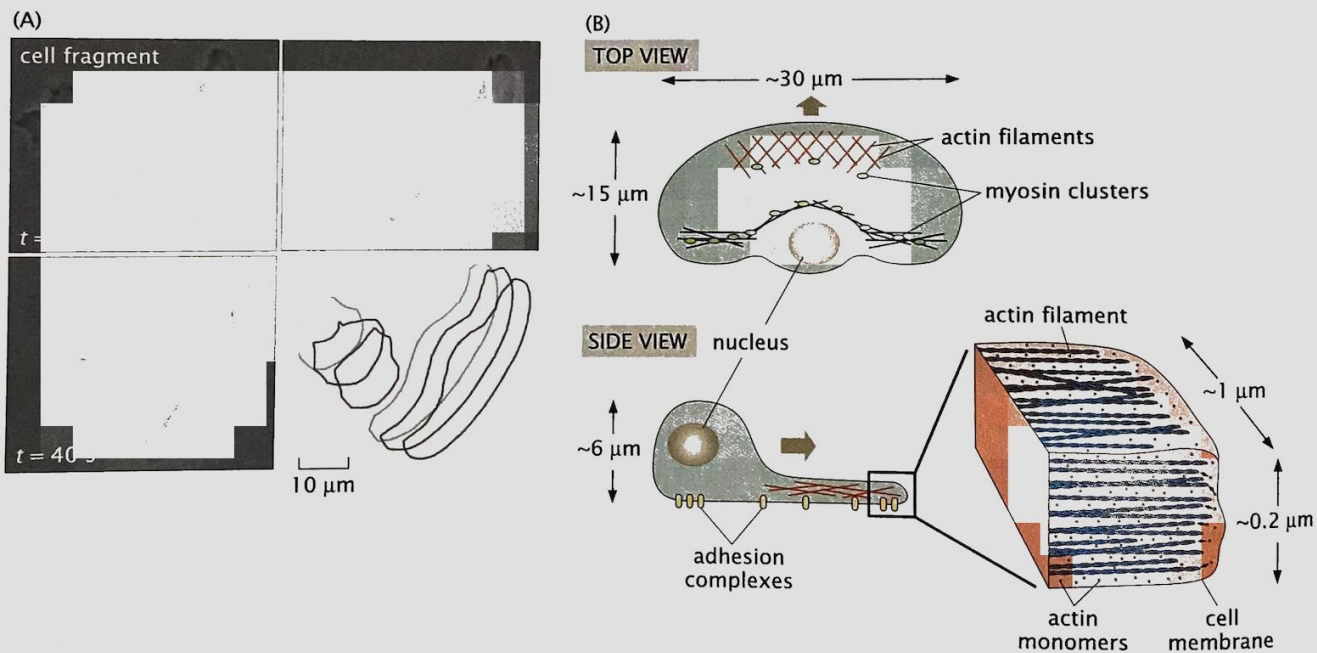
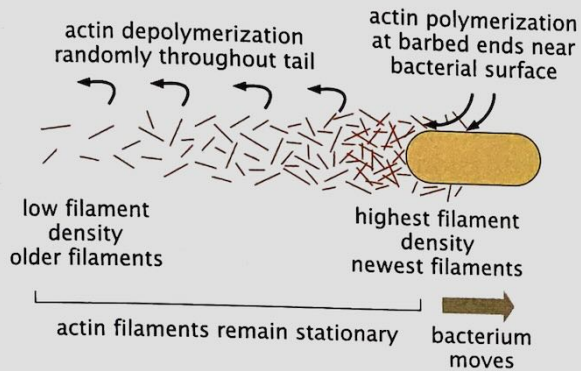


**Figure 15.2:** Actin-based crawling motility of epithelial cells. (A) This series of time-lapse images shows a single fish skin cell moving across a glass cover slip. Behind the cell an actin-rich fragment of another cell's lamellipodium is crawling autonomously without a nucleus or cell body. The frames were captured at  $20\text{s}$  intervals. The outlines show the positions of the cell and cell fragment at these time intervals. Note that they glide forward without changing shape. (B) Organization of actin filaments in the keratocyte. Seen from the top as in the microscope images, the lamellipodium is a large extension filled with a crosslinked network of actin filaments (see also Figure 14.2 on p. 547). Seen from the side, the lamellipodium is a very flat structure that drags the rounded cell body and nucleus behind it. A schematic illustration of the leading edge indicates the approximate density of actin filaments in this structure. (A, courtesy of G. Allen, K. Keren, and J. Theriot.)

(A)



(B)



(C)

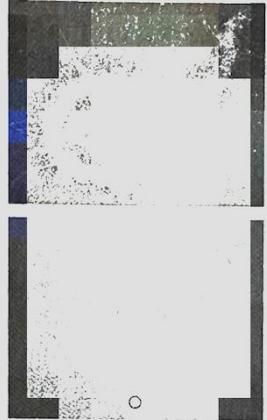


**Figure 15.3:** Actin-polymerization-driven movement of *L. monocytogenes*. (A) This series of time-lapse images shows the movement of a bacterium in a cytoplasmic extract. Phase-contrast images of the bacterium are shown on the bottom in each frame (the bacterium is indicated with an arrow) and fluorescently labeled actin is shown on the top frame. The frames were collected at 30 s intervals. (B) Schematic diagram showing the dynamics of actin filaments in the comet tail. (C) Electron micrograph of plastic bead driven by actin polymerization with schematic shown below. (A, courtesy of D. Fung and J. Theriot; C, courtesy of L. Cameron, T. Svitkina, J. Theriot, and G. Borisy.)

be abstracted from their cellular context and induced to drive the motions of synthetic beads as well.

**Estimate: The Rate of Actin Polymerization** We can use the observed rate of cell migration in the examples considered in Figures 15.2 and 15.3 to estimate the mean rate of polymerization of actin filaments. Because the motion of both the keratocyte and *Listeria* reflect the incorporation of monomers on linear actin filaments, we can make a simple estimate of the rate of polymerization through a knowledge of the speed of the cell and the size of the individual monomers that make up the actin filament. The mean velocity of a *Listeria* bacterium in a typical epithelial host cell is comparable to the speed of keratocyte migration, about  $0.2 \mu\text{m/s}$ . For each G-actin sub-unit added to the growing filament, it increases in length by approximately 3 nm (see Figure 10.29 on p. 415). If we assume that there is a perfect linear relation between the growth of individual filaments and the macroscopic motion of the cell (obviously, this is a gross oversimplification, but nevertheless provides a useful bound), then we estimate that the mean incorporation rate is

$$\frac{dN_{\text{actin}}}{dt} \approx \frac{v_{\text{cell}}}{L_{\text{monomer}}} \approx \frac{200 \text{ nm/s}}{3 \text{ nm}} \approx 70 \text{ monomers/s.} \quad (15.1)$$

Note that this rate of polymerization is very characteristic of cellular polymerization and will serve as a useful rule of thumb in subsequent discussions.



Three notes of caution are in order. First, the actual rate of polymerization is strongly dependent upon the concentration of available subunits, as we will explore in more detail later in the chapter. Second, actin polymerization is not the rate-determining step for movement of either the keratocyte or *Listeria*. Other forces such as adhesion actually limit their speeds. Third, living cells employ a legion of cytoskeleton-associated proteins to regulate the location and dynamics of actin and the other cytoskeletal filaments. Frequently, the rates of cellular events are determined by the activation and localization of these accessory proteins, rather than actin itself. Nevertheless, this estimate accurately demonstrates that cytoskeletal dynamics must be considered on time scales in which individual events may take place in only tens of milliseconds.

Besides the assembly of the actin structures at the leading edge during cell motility, another dramatic example of regulated actin dynamics is seen during cell division, when a belt of actin and myosin filaments quickly assembles around the center of a cell and contracts to pinch it in half. In the fission yeast *Schizosaccharomyces pombe*, about 30 accessory factors have been identified that modulate the assembly of actin filaments in the cleavage ring.

**Experiments Behind the Facts: Taking the Molecular Census** As stated above, rates for cytoskeletal reactions depend upon the concentrations of the proteins involved. Many proteins are not uniformly distributed throughout the cell, and we need to know the local concentration rather than the global average concentration of the protein of interest. For these purposes, merely knowing the number of molecules per cell is not enough; we must also know their spatial distribution. The combination of fluorescence microscopy with other quantitative techniques permits this kind of measurement.

An example of a census of actin-related proteins is shown in Figure 15.4. It is first necessary to determine the total concentration of each protein and then to characterize the distribution of the protein within individual cells. For a large number of proteins believed to play roles in cell division, *S. pombe* strains were generated in which exactly one protein of interest was fused to a yellow fluorescent protein, YFP. In order to determine the number of molecules of each tagged protein present in the cells, the average protein concentration can be measured using a quantitative technique such as Western blotting. In a Western blot, the proteins from a large population of cells are all run out together on a gel and then probed with an antibody. A specific antibody against YFP recognizes all of the tagged proteins with equal affinity, and the Western blot signal can be calibrated against a known dilution of purified YFP. Dividing this by the number of cells loaded on a gel gives a measurement of the average concentration of each tagged protein per cell. Having calibrated the actual number of molecules per cell using the Western blot, the measured fluorescence intensity (observed either by fluorescence microscopy or by flow cytometry) can be related to an absolute scale of cytoplasmic protein concentration. Finally, local concentrations can be determined from the fluorescence microscopy images. Proteins involved in building the cytokinetic furrow (plane of cell division) are concentrated up to 100-fold on the furrow relative to their global abundance.



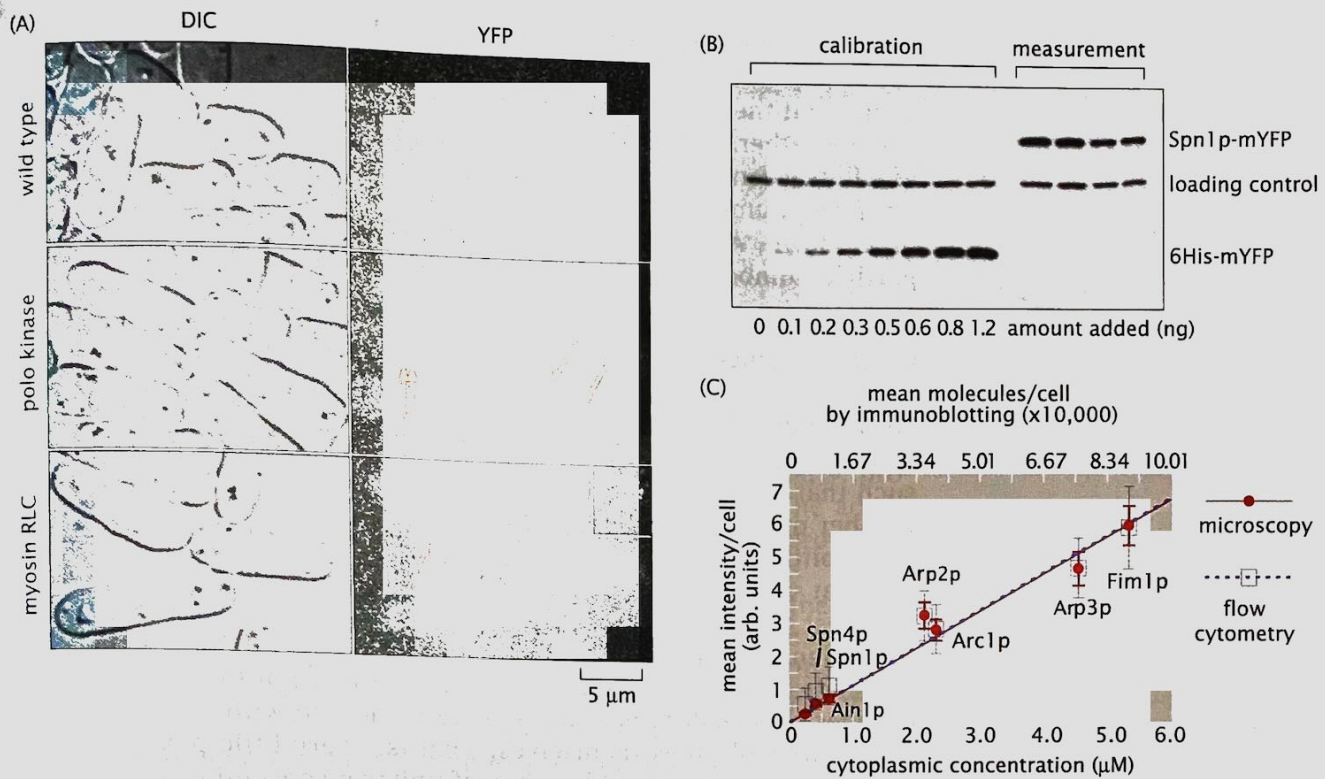


**Figure 15.4:** Calibration and quantitation of cell-division-associated proteins in the fission yeast *S. pombe*. (A) Wild-type yeast cells, clearly visible as individuals by differential interface contrast microscopy, have no fluorescent signal in the YFP channel. Polo kinase is not visible in most cells, but, in two cells caught in the process of chromosome segregation, the kinase is seen concentrated in pairs of dots (yellow arrows). The myosin regulatory light chain accumulates in a narrow ring as seen in the cell at the bottom of the image (blue arrow), immediately before the cell divides. At a slightly earlier stage in the cell cycle, myosin regulatory light chain begins to accumulate near the presumptive division site in a loose band of dots (red arrow). (B) The average concentration of each protein fusion can be measured using calibrated Western blots. On the left-hand half of the gel, known amounts of purified YFP protein are loaded together with a control protein present in the same amount in every lane. On the right-hand part of the gel, four replicate measurements are made for a single YFP-tagged protein. The amount of the tagged protein is determined by comparing the intensity of the bands with the calibration curve. (C) The number of molecules per cell determined by immunoblotting is linearly related to the average fluorescence intensity per cell measured by flow cytometry or fluorescence microscopy. (A–C, adapted from J.-Q. Wu and T. D. Pollard, *Science* 310:310, 2005.)

## 15.2 A Chemical Picture of Biological Dynamics

We have given a few qualitative descriptions of cases where understanding rates of transformation is critical to understanding biological processes, with examples ranging from the energy budget of ATP in the cell to the dynamics of the cytoskeleton. We now turn to building the quantitative toolkit that will allow us to treat these cases rigorously by tracking the concentrations of the different molecular players over time. A quantitative theory of such reactions must ultimately answer three key questions about all of the molecular participants: how many molecules are there, where are they, and when are they there? To that end, we will first focus on the general ideas associated with the rate equation paradigm, and then provide several different case studies, including the dynamics of ion channel gating and the time evolution of cytoskeletal filaments.

### 15.2.1 The Rate Equation Paradigm

The starting point for our discussion is the idea of a chemical concentration. Recall that the concentration tells us the number of molecules

of a given species per unit volume (see Figure 13.9 on p. 516). The conventional reason for using a concentration rather than explicitly calling out the *number* of molecules is that the concentration is applicable whether we talk about a drop of water or an entire lake, though, as will be seen when discussing the Gillespie algorithm in Chapter 19, when the number of molecular players is very small these ideas can break down. As we will see below, concentrations (and not absolute particle numbers) often dictate the rates of chemical reactions.

### Chemical Concentrations Vary in Both Space and Time

For the purposes of the present discussion, we now imagine that the concentration of the  $i$ th species varies with both position and time such that we think of the concentration as  $c_i(\mathbf{r}, t)$ , which tells us the number of molecules of type  $i$  per unit volume at position  $\mathbf{r}$  at time  $t$ . Exploiting a definition of concentration as a “field variable” (a quantity that varies in space) anticipates the fact that the chemical state of a test tube or a cell can develop spatial nonuniformity (that is, dependence on  $\mathbf{r}$ ) and time variation. The assumption that makes these ideas tolerable is that the spatial variation of the concentration changes over distances that are large compared with the mean spacing of the molecules themselves. That is, every little box within the overall volume behaves like a box of uniform concentration.

We note that in the context of a living cell, there may be reasons to doubt the validity of the concentration idea itself since (i) the number of molecules can be exceedingly small and (ii) such molecules can be localized to membranes or particular organelles. Thus it is important to bear two things in mind: first, local concentration rather than global concentration is the appropriate parameter for cases where molecules are confined to particular organelles or regions, and, second, for those cases where actual molecular numbers are small, it will be important to consider the stochastic behaviors of individual trajectories rather than global averages. With these provisos, we forge ahead.

### Rate Equations Describe the Time Evolution of Concentrations

We begin with the simplest case, in which we assume that the concentration at one point in space is identical to that at another. As a result, we drop the label  $\mathbf{r}$  in our description of the concentration and focus only on  $c_i(t)$ , which changes over the course of time as a result of the reactions that link the various reactants,  $\{c_j\}$ . We introduce the notation  $\{c_j\}$  as shorthand for the set  $(c_1, c_2, c_3, \dots, c_n)$  where each subscript refers to a different species. The fundamental postulate of the rate equation paradigm is that we can write the time evolution of the concentration in the form of a differential equation as

$$\frac{dc_i(t)}{dt} = f(\{c_j\}; \{k_i\}), \quad (15.2)$$

where  $f(\{c_j\}; \{k_i\}) = f(c_1, c_2, \dots, c_n; k_1, k_2, \dots, k_m)$ . These various concentrations  $c_1, c_2, \dots, c_n$  are for all of the species implicated in the reactions of interest and the parameters  $k_i$  are “rate constants” that dictate how fast the various reactions go. Equation 15.2 says that the concentration of the  $i$ th species changes in time. How much it will change depends upon the concentrations of all of the various other species that couple to  $c_i$ . To make these ideas precise, we now

consider explicit examples of different types of reaction that take  $f(\{c_j\}; \{k_i\})$  from abstract to concrete form.

### 15.2.2 All Good Things Must End

#### Macromolecular Decay Can Be Described by a Simple, First-Order Differential Equation

One of the key physical processes that must be considered when trying to endow the function  $f(\{c_j\})$  with real content is the idea that macromolecules decay and are degraded. For example, if we consider the mRNA within a cell, these molecules are generally short-lived in comparison with the average division time of the cell. Similarly, proteins in the cell have a characteristic tendency to decay. The actual lifetime of an individual protein may vary from one kind of protein to another and may be regulated within the cell.

For these decay reactions, just as for radioactive decay, the material does not vanish but rather is transformed into something else. Degraded mRNA is broken down into individual nucleotides and degraded proteins are broken down into individual amino acids. For the purposes of our discussion on rates of decay reactions, we will begin by ignoring these complexities and instead consider the concentration of only one species at a time.

Our principal biological example in this section will be the chemical reaction that lies at the heart of photosynthesis and also vision. A small organic molecule called retinal, illustrated in Figure 15.5, can exist in two slightly different conformational forms. As found in its natural environment associated with a protein in the membrane of photosynthetic archaea, the lower-energy form of retinal, or ground state, is referred to as “all-trans-retinal” because of the arrangement of the double bonds in its long tail. A second form, 13-cis-retinal, exists in a slightly higher-energy state. To go from the all-trans form to the 13-cis form, one of the carbon–carbon double bonds must undergo a 180° rotation introducing a kink in the middle of the molecule’s tail. In nature, retinal and related molecules can undergo this conformational change (also called an isomerization reaction) when they collide with a photon carrying the appropriate energy. Absorption of the energy from the photon enables retinal to overcome the significant energy barrier for rotation of this double bond as illustrated in Figure 15.5(B). Given sufficient time, the slightly higher-energy 13-cis-retinal will decay back to the lower-energy form of all-trans-retinal.

This tiny conformational change is exploited by cells in several remarkable ways. In photosynthetic archaea, retinal is embedded at the heart of a large transmembrane protein called bacteriorhodopsin. The photon-induced kinking of the retinal is amplified by the protein to generate a large-scale conformational change that eventually results in the transport of a single hydrogen ion from the inside of the cell to the outside of the cell. Thus, the energy of the photon has been converted into an electrochemical transmembrane gradient, which can be used by the archeon to generate ATP, to spin its flagella, and for any other purpose it desires. In the human retina, protein homologs of bacteriorhodopsin are found in light-sensitive rod and cone cells. Here a slightly different isomerization of retinal (from the 11-cis form to the all-trans form) initiates a signal transduction cascade that triggers neurons to communicate the change in state to the visual cortex of the brain, where we perceive retinal isomerization as light.

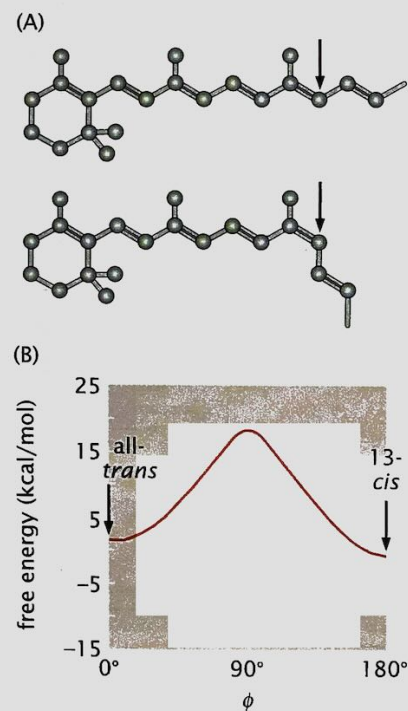


**Figure 15.5:** The conformational change of retinal. (A) The all-trans form of retinal, shown at the top, is its lowest-energy state. The 13-cis form, shown at the bottom, is formed by rotation around the atom indicated with the arrow. This rotation is commonly caused by absorption of a photon. (B) The calculated energy landscape for retinal as a function of the degree of rotation around the carbon atom reveals a large energy barrier between the cis and trans forms. (B, adapted from A. Hermone and K. Kuczera, *Biochemistry* 37:2843, 1998.)

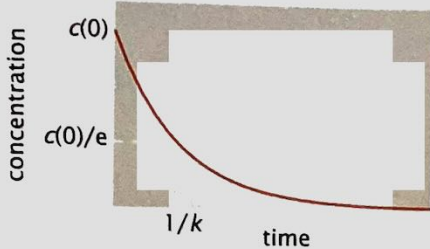


**Figure 15.6:** The number of molecules as a function of time during a decay process. The time scale  $1/k$  sets the time it takes before the concentration has decayed to  $1/e$  of its initial value.

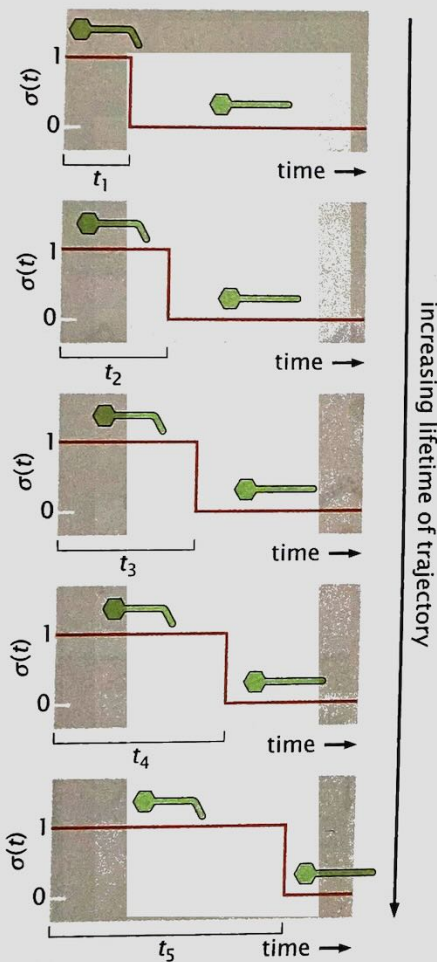


**Figure 15.7:** Schematic showing the class of microscopic trajectories for a system undergoing simple isomerization/decay dynamics. The two states of the system are labeled by 1 and 0, and hence a given trajectory is characterized by some waiting time in the 1 state followed by a fast decay to the 0 state. The transition itself is assumed to be very fast relative to the waiting time. The set of trajectories shown here provides a few representative examples. The waiting time  $t_i$  is actually a continuous variable, so there is a continuum of allowed trajectories.

Decay reactions like the conversion of 13-cis-retinal into all-trans-retinal can be captured very simply using equations of the form of Equation 15.2. In particular, for the case in which we are interested in the simple decay of a given reactant, we have  $f(c; k) = -kc$ , which says that the rate of decay of the reactant is proportional to how much reactant there is around. The parameter that characterizes that decay rate for a given molecular species is  $k$  and the evolution equation itself is

$$\frac{dc(t)}{dt} = -kc(t). \quad (15.3)$$

Note that the constant  $k$  that parameterizes the rate of decay has units of  $1/\text{time}$ .

This linear differential equation can be solved by recourse to the method of separation of variables (see Equation 13.58 on p. 530) and results in a solution of the form  $c(t) = c(0)e^{-kt}$ , yielding a time-dependent concentration profile of the form

$$c(t) = c_0 e^{-t/\tau}, \quad (15.4)$$

where  $c_0$  is the initial concentration (that is,  $c(0) = c_0$ ) and we have defined a characteristic time  $\tau = 1/k$ . The time evolution in the concentration of molecules that suffer such decay is shown in Figure 15.6. This simple calculation shows that if we start out with some initial concentration  $c_0$ , this concentration will steadily decline over time with an average exponential profile like that shown in the figure and symbolized in Equation 15.4. A cautionary note is in order: the use of rate equations like those advocated here focuses on the average values of quantities of interest. This automatically deprives us of deeper contact with fluctuational quantities. This is one reason we now turn to considering these processes from the single-molecule perspective.

### 15.2.3 A Single-Molecule View of Degradation: Statistical Mechanics Over Trajectories

#### Molecules Fall Apart with a Characteristic Lifetime

As noted above, the simplest mathematical description of decay dynamics is founded upon introducing a characteristic decay constant. It is of interest to examine this decay constant more deeply from both a phenomenological and a microscopic perspective. We adopt the view that the molecule can undergo any of an infinite number of different microscopic trajectories. The idea is that when the system has not yet decayed it is in a state labeled with a 1 and when it has decayed it is labeled with a 0. Here we are generalizing the equilibrium ideas of Chapter 7 to the dynamical case where we consider the transitions between the two states over time. An example of this class of trajectories is shown in Figure 15.7.

Mathematically, we label these trajectories  $\sigma_i(t)$ , where the trajectory is defined as

$$\sigma_i(t) = \begin{cases} 1 & \text{if } t < t_i, \\ 0 & \text{otherwise,} \end{cases} \quad (15.5)$$

where the time  $t_i$  is the waiting time associated with the trajectory of interest. The role of the constant  $k$  (or alternatively, of  $\tau = 1/k$ ) is to

characterize the *average* lifetime of the macromolecule of interest. Because the rate constant  $k$  has units of inverse time (for example,  $\text{s}^{-1}$ ) as it describes the probability that something will happen per unit time, its reciprocal  $\tau$  simply has units of time and can be thought of intuitively as dictating the average lifetime of the molecule. That is, a given macromolecule, such as a mRNA, can decay after a waiting time of one second or one minute or one week. However, when we consider a huge collection of such molecules, it makes sense to speak of an average lifetime associated with these molecules, and that is what the decay constant captures.

We can use this trajectory picture with our “trajectories-and-weights” approach introduced in Figure 13.14 (p. 520). We discretize time into  $N$  intervals of length  $\Delta t$  (so the total time  $t = N\Delta t$ ) and then find the probability of a given trajectory by multiplying the probabilities of what happens at each time step over the entire trajectory. For example, if the molecule survives for  $N$  time steps and decays on the  $(N+1)$ th time step, then the probability of that process is

$$p(t)\Delta t = \underbrace{(1 - k\Delta t) \times (1 - k\Delta t) \times \cdots \times (1 - k\Delta t)}_{N \text{ time steps}} \times k\Delta t, \quad (15.6)$$

where  $k\Delta t$  is the probability of a decay during any time step and  $1 - k\Delta t$  is the probability of no decay at a given time step. The function  $p(t)$  is a probability density and requires that we compute  $p(t)\Delta t$  to compute the probability that the decay occurs between time  $t$  and  $t + \Delta t$ . If we use the fact that  $\Delta t = t/N$ , this result can be rewritten as

$$p(t)\Delta t = (1 - k\Delta t)^N k\Delta t = \left(1 - \frac{kt}{N}\right)^N k\Delta t \approx ke^{-kt}\Delta t, \quad (15.7)$$

where we have used the identity that  $e^{-x} = \lim_{N \rightarrow \infty} (1 - x/N)^N$ . This result tells us that once we have set the mean lifetime ( $\tau = 1/k$ ), the probability of decay in the time interval between  $t$  and  $t + \Delta t$  is

$$p(t)\Delta t = \frac{1}{\tau} e^{-t/\tau} \Delta t. \quad (15.8)$$

### Decay Processes Can Be Described with Two-State Trajectories

Another way of illustrating the trajectory perspective for decay processes is to exploit the maximum-entropy approach introduced in Section 6.1.5 (p. 253). Recall that each decay process is characterized by a trajectory corresponding to how long the system is in state A before decaying to state B. It is convenient to characterize the molecular state with the discrete index 1 for state A and 0 for state B. Our aim here is to use the information-theoretic approach to statistical mechanics introduced in Section 6.1.5 (p. 253) to obtain the probability distribution on these trajectories. Just as our discussion in Chapter 6 showed several ways to obtain the Boltzmann distribution, our present discussion illustrates several distinct ways of deriving the waiting time distribution,  $p(t)$ .

We are interested in the probability  $p(t)$ , which signifies the probability of a microtrajectory with lifetime  $t$ , precisely the same quantity considered in Equation 15.8. The only information about the overall process that we invoke in our analysis is that the average lifetime

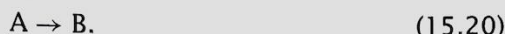
Hence, our second Lagrange multiplier  $\mu$  is now determined as  $\mu = 1/\tau$ . Substituting this result into Equation 15.16 yields  $p(t) = (1/\tau)e^{-t/\tau}$ , leading in turn to the result that the probability that the decay will occur between times  $t$  and  $t + \Delta t$  is given by

$$p(t)\Delta t = \frac{1}{\tau}e^{-t/\tau}\Delta t. \quad (15.19)$$

We will come back to this in the context of molecular motors when analyzing the different lifetimes of a motor's internal states (see Section 16.2.3 on p. 647).

### Decay of One Species Corresponds to Growth in the Number of a Second Species

The reactions we have been thinking about are described by the simple chemical formula



This kind of process is depicted schematically in Figure 15.8 for the example of retinal. Thus far, we have considered only the fate of species A, but of course in the real reaction the number of molecules of the product species B also changes with time and the time-dependent equations describing the fates of A and B are inextricably linked to one another. In this case, for every decrease in the number of A molecules, we have a corresponding increase in the number of B molecules, which implies the constraint

$$c_A(t) + c_B(t) = c_0. \quad (15.21)$$

Indeed, the dynamics of these two species as embodied in Equation 15.21 is nothing more than an expression of mass conservation. The condition of mass conservation implies that

$$\frac{dc_A}{dt} = -\frac{dc_B}{dt} = -kc_A. \quad (15.22)$$

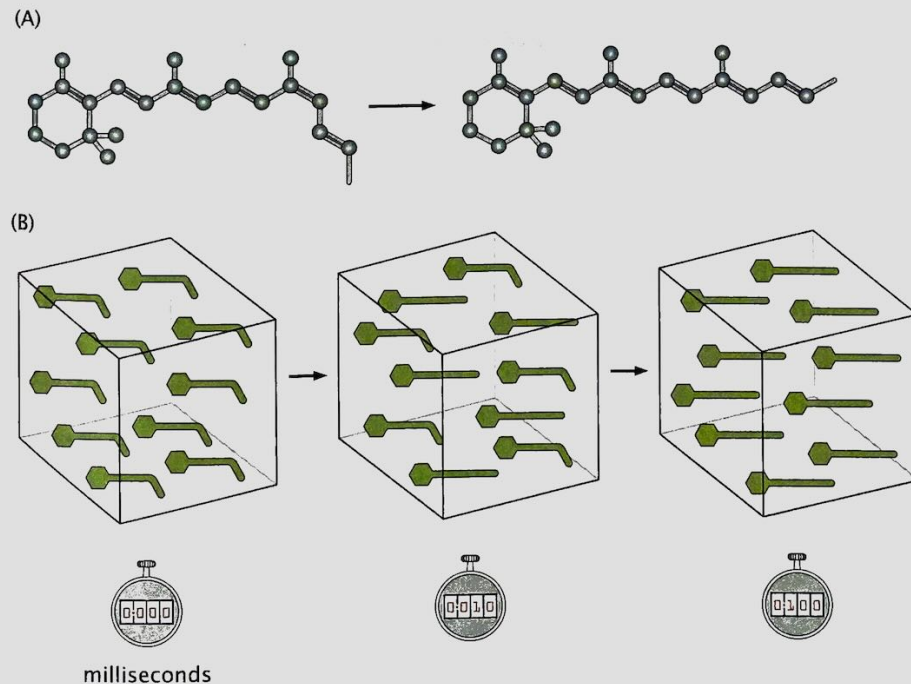


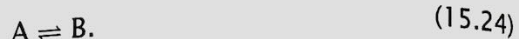
**Figure 15.8:** Different views of the isomerization process. (A) Schematic of an isomerization process where species A is decaying into species B. In this case, we use the two forms of retinal described earlier in the chapter to characterize the process. (B) Schematic of the change in the populations of the two species over time.

If we consider the situation where initially all of the molecules are A molecules, then we have  $c_A(0) = c_0$  and  $c_B(0) = 0$ . From our earlier solution of the decay problem, it is now straightforward to write down the time evolution of both species. Using the mass conservation condition given in Equation 15.21, we find

$$\frac{dc_B}{dt} = kc_A = k[c(0) - c_B] \Rightarrow c_B(t) = c_0(1 - e^{-kt}). \quad (15.23)$$

The time evolution of both populations under these initial conditions is indicated schematically in Figure 15.8, and the reader is asked to flesh out this solution and make the corresponding plots in the problems at the end of the chapter.

The same ideas introduced above can be used just as well for examining the reversible reaction



In this case, the rate equations of interest can be written as

$$\frac{dc_A}{dt} = -k_+c_A + k_-c_B \quad (15.25)$$

and

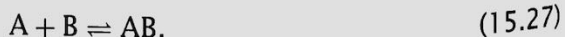
$$\frac{dc_B}{dt} = -\frac{dc_A}{dt}, \quad (15.26)$$

with the constraint of mass conservation of the form given in Equation 15.21. Equation 15.25 says that the change in concentration of species A comes from two sources, namely, (i) the decay of A into B with rate constant  $k_+$  and (ii) the decay of B into A with rate constant  $k_-$ . In this case, the long-time behavior is nonzero concentrations of both A and B, with their ratio dictated by the ratio  $k_+/k_-$ . The details of this analysis are left to the reader in the problems.

#### 15.2.4 Bimolecular Reactions

##### Chemical Reactions Can Increase the Concentration of a Given Species

Decay and isomerization are only a limited subset of the repertoire of interesting biochemical transactions. Indeed, these reactions are unusual in that there is only one molecule involved; this one molecule may change its state, but does not explicitly interact with other molecules. In general, the more interesting cases are those in which two different reactants come together to form some third product. In these cases, the function  $f(\{c_j\})$  must have contributions coming from the presence of interactions between the different reactants. In particular, we now consider reactions of the form



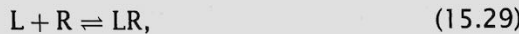
As before, our interest is in finding a description that provides us with the concentrations of both reactants and products as a function of time.

Intuitively, we can argue that the contribution of the association reaction to the overall concentration of the products can be written as

$$\frac{dc_{AB}(t)}{dt} = k_{AB} c_A c_B, \quad (15.28)$$

where  $k_{AB}$  is a constant that reflects the rate of association of A and B molecules. Conceptually, this equation says that A and B molecules come together to form AB molecules and the rate at which they do so is proportional to the probability that A's and B's are at the same place (that is, their concentrations). Note that bimolecular reactions lead to a new feature in our description. In particular, we note that the dynamical equations of different species are coupled. In our earlier treatment of decay reactions, the equation for  $c_A(t)$  made no appeal to the concentrations of other species. In the present case, changes in the concentration of one species are accompanied by a concomitant change in the concentrations of other species. Mathematically, this amounts to the fact that the differential equations for the system are *coupled* (in more than the simple way revealed in Equation 15.22).

To see how this works more concretely, we return to one of our workhorse problems, namely, ligand-receptor binding, and now explicitly consider how the system changes over time. We consider a ligand and receptor whose concentrations are  $[L]$  and  $[R]$ , which are either free in solution or bound in the LR complex, whose concentration is  $[LR]$ . To model the reaction



we consider a lattice model as shown in Figure 15.9, in which there are a total of  $\Omega$  distinct "lattice" sites,  $L$  ligands, and  $R$  receptors. We treat the solution as an ideal solution of ligand and receptor where the probability of occupancy of an elementary box by ligand is  $L/\Omega$  and the probability of occupancy of a box by receptor is  $R/\Omega$ . Furthermore we assume that for L and R to form a complex, they must be in the same box. Given these assumptions, in time  $\Delta t$ , the change in

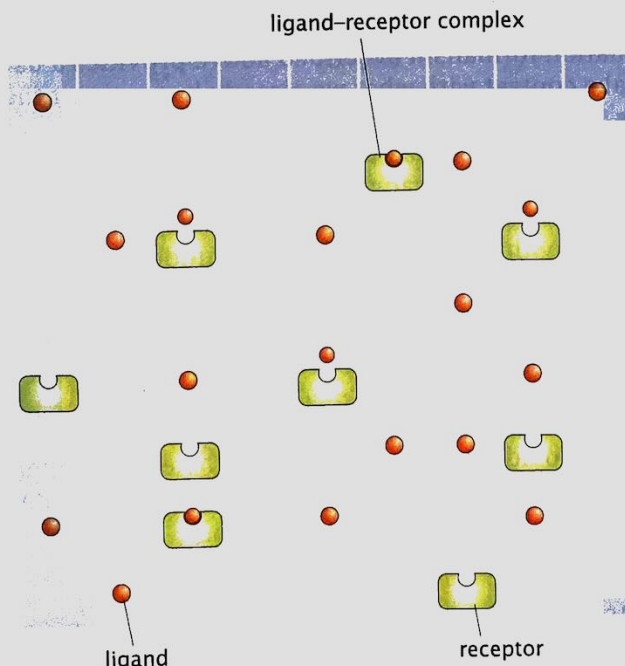


**Figure 15.9:** Lattice model of ligand-receptor binding dynamics. The system is divided up into  $\Omega$  distinct boxes. There are  $L$  ligands and  $R$  receptors in solution and the binding reaction between them to form the complex LR can occur when a ligand and receptor are found at the same lattice site. When a ligand and receptor are found in the same box, the probability that they will react to form LR in time  $\Delta t$  is given by  $k'_{\text{on}} \Delta t$ .

the number of ligand-receptor complexes due to binding of ligand to receptor can be written as

$$\Delta N_{LR} = \underbrace{-(k_{off}\Delta t)N_{LR}}_{\text{decay term}} + \left( \underbrace{\frac{\Omega}{\text{no. of boxes}}}_{\text{box occupancy prob.}} \times \frac{N_L}{\Omega} \frac{N_R}{\Omega} \times (k'_{on}\Delta t) \right), \quad (15.30)$$

where the first term is the decay process discussed earlier (see Section 15.2.2 on p. 581), while the second term represents the rate at which LR is produced and is obtained by working out the rate per elementary box times the total number of such boxes;  $k'_{on}$  is the rate at which ligand-receptor pairs that are colocalized in the same elementary box transform to a ligand-receptor complex.

This result can be recast in the more familiar differential form by dividing the left- and right-hand sides by  $\Delta t$  and then by the volume  $\Omega v$ , where  $v$  is the volume of each elementary box in our lattice model. In particular, we have

$$\frac{d}{dt} \left( \frac{N_{LR}}{\Omega v} \right) = -k_{off} \left( \frac{N_{LR}}{\Omega v} \right) + \frac{\Omega}{\Omega v} \frac{N_L}{\Omega v} \frac{N_R}{\Omega v} v^2 k'_{on}, \quad (15.31)$$

where in the second term on the right we have divided and multiplied by  $v$  twice in order to convert to concentration variables such as  $[L] = N_L/\Omega v$ ,  $[R] = N_R/\Omega v$ , and  $[LR] = N_{LR}/\Omega v$ . These manipulations transform Equation 15.30 into

$$\frac{d[LR]}{dt} = -k_{off}[LR] + k'_{on}[L][R], \quad (15.32)$$

where the bimolecular on-rate is related to the lattice model rate constant by  $k'_{on} = v k_{on}$ , and has units of  $M^{-1} s^{-1}$ . This heuristic derivation shows how to link simple lattice models with macroscopic rate equations defined in terms of concentration variables.

### Equilibrium Constants Have a Dynamical Interpretation in Terms of Reaction Rates

The rate equation formalism described above provides a useful opportunity to make contact with what we already know about the equilibria of reactions. In particular, by definition, equilibrium is a reflection of the fact that the reaction has reached a steady state where the concentrations are no longer changing over time because the forward flux in the reaction exactly balances the backward flux. It is important to note that individual molecules are still undergoing the reactions, but the net number of transformations in each direction is equal, so the overall concentration does not change. We can express this idea mathematically as  $d[LR]/dt = 0$ , resulting in

$$-k_{off}[LR]_{eq} + k'_{on}[L]_{eq}[R]_{eq} = 0. \quad (15.33)$$

This equation provides a relation between the equilibrium concentrations ( $[L]_{eq}$ ,  $[R]_{eq}$ ,  $[LR]_{eq}$ ) and the relevant rate constants, namely,

$$K_d = \frac{[L]_{eq}[R]_{eq}}{[LR]_{eq}} = \frac{k_{off}}{k'_{on}}. \quad (15.34)$$

Using our rate equation picture, we have recovered the law of mass action derived using statistical mechanics in Section 6.3 (p. 267) where

we demonstrated that  $K_d$  is the concentration at which  $p_{\text{bound}} = 1/2$ . This equation demonstrates the connection between the equilibrium concentrations and the associated kinetic rate constants. However, as indicated schematically in Figure 15.10, the rate picture allows us to say much more than what the terminal, privileged (equilibrium) state will be. The dynamical picture captured by the rate equations permits us to examine the variation in the concentrations over time for different choices of their initial values (that is, at time  $t = 0$ ).

### 15.2.5 Dynamics of Ion Channels as a Case Study

An interesting application of the ideas developed so far is the dynamics of ion channels. In Chapter 7, we discussed ion channels as an example of a real biological system that can be fruitfully viewed using the two-state paradigm because in the simplest picture, they exist only in open or closed states (see Figure 7.2, p. 283). There we considered channel behavior only from an equilibrium perspective and now we are ready to turn to the question of rates. For example, when the membrane of a nerve cell is depolarized, how long does it take for the voltage-gated calcium channels to open, and how does the time-dependent behavior of the ion distribution along the whole membrane depend on the behavior of the individual channels themselves? Our goal is to write a rigorous description that relates the trajectories of individual channels, which are intrinsically binary, to the

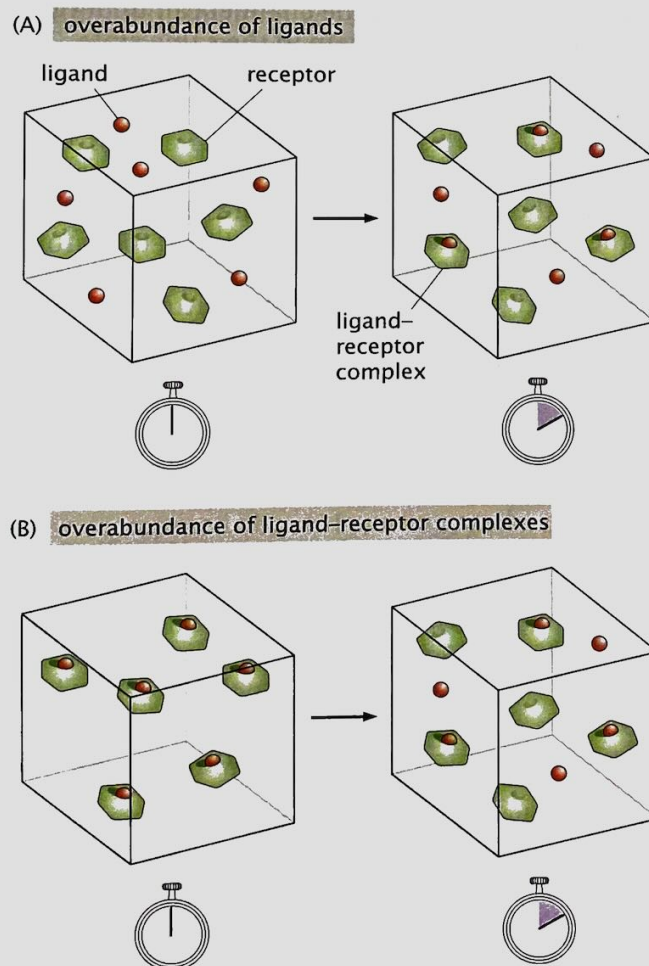


**Figure 15.10:** Direction of reaction.  
 (A) Time evolution of the system in the case in which the initial concentrations of  $[L]$  and  $[R]$  are in excess of their equilibrium concentrations. (B) Time evolution of the system in which the initial concentration of  $[LR]$  is in excess of its equilibrium concentration.

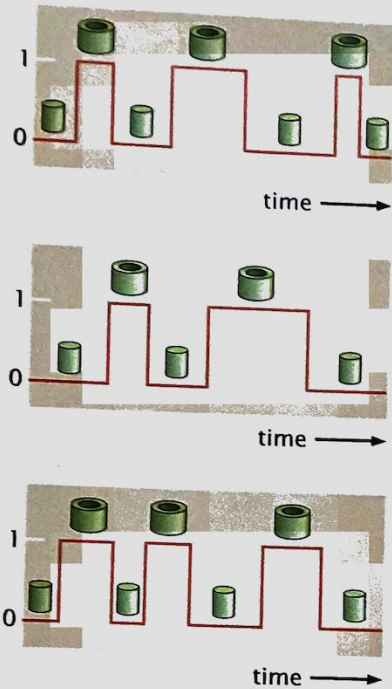


**Figure 15.11:** Ion channel trajectories. Three representative examples of the time evolution of a two-state ion channel that switches back and forth between the closed and open states. For simplicity, we assume that the switching itself is *instantaneous* in comparison with the time spent in either of the two states. The icons represent the open and closed states.

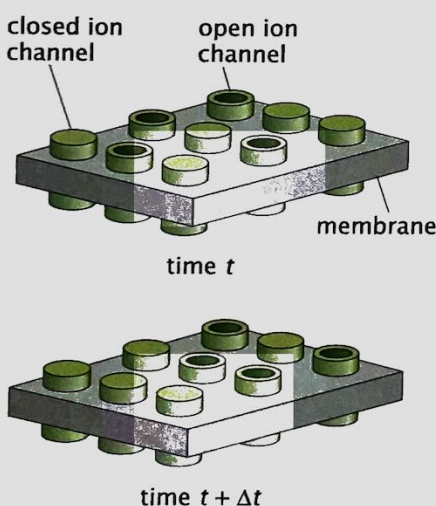


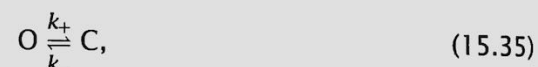
**Figure 15.12:** Channel gating kinetics. A patch of membrane with a collection of ion channels, some of which are open, some of which are closed. At every time step, channels can either switch their state or stay in the same state.

overall behavior of a large-scale system that may have an analog-like response. In addition, we explore a probabilistic description of how the behavior of identical channel molecules may differ over time. We will model the channel as existing in only two states, open and closed, with only a single relevant transformation reaction converting one state into the other. This will be a warm-up problem for more complex systems later in the chapter that involve more molecular species and more complex transformations.

### Rate Equations for Ion Channels Characterize the Time Evolution of the Open and Closed Probability

Examples of the microtrajectories available to individual channels are shown in schematic form in Figure 15.11. Our goal is to write a kinetic description that allows us to classify and analyze different trajectories. One quantity we might like to use to characterize ion channel dynamics is the probability that, if we start in the open state at time  $t = 0$ , it will still be open a time  $\tau$  later.

To exploit our rate equation paradigm for the problem of ion channel dynamics, we appeal to Figure 15.12. The idea is that we have a patch of membrane that is occupied by a total of  $N$  distinct two-state channels. Our goal is to write a rate equation that characterizes the time evolution of the probability of being in the open state and the way we will do this is to compute  $N_O(t)/N$  (where  $N_O(t)$  is the number of open channels at time  $t$ ), which will effectively determine that probability. We adopt a strategy in which time is discretized into steps of length  $\Delta t$  and, at each time step, the channel can undergo a transition from its current state or it can remain in the same state. The “reaction” of interest is of the form



where  $O$  signifies the open state,  $C$  signifies the closed state and  $k_+$  and  $k_-$  are the rate constants that determine the probability of a change of state during a given time step. The change in the number of open channels in a given time step can be written as

$$\Delta N_O = -k_+ N_O \Delta t + k_- N_C \Delta t. \quad (15.36)$$

If we divide both sides by  $\Delta t$ , we find the rate of change in the number of open channels as

$$\frac{\Delta N_O}{\Delta t} = -k_+ N_O + k_- N_C, \quad (15.37)$$

which can be further simplified by dividing this equation by  $N$  itself and using  $p_O = N_O/N$  and  $p_C = N_C/N$ . If we examine the limit as  $\Delta t \rightarrow 0$ , this results in the differential equation

$$\frac{dp_O}{dt} = -k_+ p_O + k_- p_C. \quad (15.38)$$

If we now exploit the fact that  $p_O + p_C = 1$ , which amounts to the statement that the channels are either open or closed (that is, it is a two-state system), this may be rewritten as

$$\frac{dp_O}{dt} = -k_+ p_O + k_- (1 - p_O). \quad (15.39)$$

This equation is more transparent if written in the form

$$\frac{dp_0}{dt} = -(k_+ + k_-)p_0 + k_- \quad (15.40)$$

In particular, we can solve this equation by resorting to separation of variables and by adding a constant term, resulting in

$$p_0(t) = \frac{k_-}{k_+ + k_-} + Ae^{-(k_+ + k_-)t}. \quad (15.41)$$

The specific solution cancels off the constant term in the differential equation and the exponential term captures the time dependence. If we now exploit the initial condition that  $p_0(0) = 1$  (that is, all the channels are open at  $t = 0$ ), we can determine the constant  $A$ , resulting in

$$p_0(t) = \frac{k_-}{k_+ + k_-} + \frac{k_+}{k_+ + k_-} e^{-(k_+ + k_-)t}. \quad (15.42)$$

The dynamics of the channel is usefully characterized using this probability, which we will show below can also be thought of as providing the *correlation function*. In particular, this solution tells us how to view trajectories like those given in Figure 15.11 with particular reference to how long the channel stays in the closed and open states between switching events. Consider a single-molecule experiment in which we observe a channel switching back and forth between the closed and open states (experimental data of this kind are shown in Figure 7.2 on p. 283). Imagine we start our stopwatch when the protein is in the open state, and we record the state of the protein in time, assigning 0 to the closed state and 1 to the open state. This will result in a random telegraph signal  $\sigma(t)$  like that shown schematically in Figure 15.11. Our task is to compute the correlation function  $\langle \sigma(0)\sigma(t) \rangle$ . The average can be computed by repeating the experiment over and over again; the figure shows the hypothetical outcomes of three such experiments. Alternatively, we could watch a single channel over a long time period and compute a time average. In the case of a stationary process (one that looks the same whenever we view it), the two procedures give the same result. For a stationary process, the random graph you get by shifting  $\sigma(t)$  is just as good as the original, that is, it is drawn from the same distribution.

For a *given* process  $\sigma(t)$ , the quantity  $\sigma(0)\sigma(t)$  is either 1 or 0. The average  $\langle \sigma(0)\sigma(t) \rangle$  is therefore equal to the probability of  $\sigma(t)$  being 1, *conditioned on*  $\sigma(0)$  being equal to 1. But this is precisely the probability  $p_0(t)$  that we computed above. Experimentally, one way to evaluate these probabilities is to examine channel trajectories like those shown in Figure 7.2 (p. 283) and to make a histogram of the number of times each waiting time (in the interval  $t$  and  $t + \Delta t$ , where  $\Delta t$  is the bin size) appears. Experimental data of this variety for a sodium channel are shown in Figure 15.13.

### 15.2.6 Rapid Equilibrium

Having flexed our muscles with relatively simple two-state ion channels, we are now ready to turn to more complex biological systems that involve multiple transformations. One useful exercise we are now prepared for is to return to the discussion of Section 5.2.1 (p. 200). The goal of that discussion was to assess the circumstances under

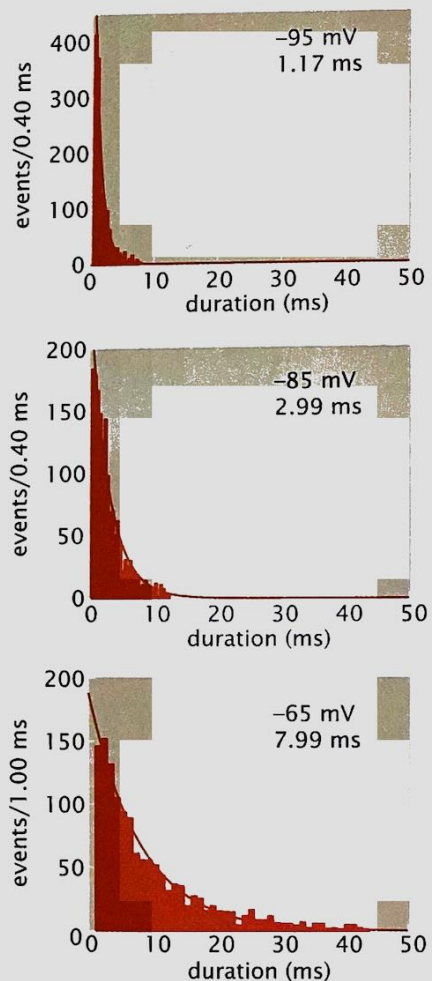


**Figure 15.13:** Measured channel gating kinetics. Each histogram shows the number of events observed for the open-state lifetime for a voltage-gated sodium channel. The frequencies shown on the y-axis are given as number of events per bin size (measured in milliseconds). Note that the bin size is larger for the bottom graph. The three histograms correspond to different membrane voltages as indicated in the figure. The average lifetime  $\tau$  is shown for each voltage. (Adapted from B. U. Keller et al., *J. Gen. Physiol.* 88:1, 1986.)